Biotribology 26 (2021) 100168

Contents lists available at ScienceDirect

Biotribology

journal homepage: www.elsevier.com/locate/biotri

Using nanoparticles to prevent enamel wear

Yan Chen [a], Bradley T. Simon [b], Lynne A. Opperman [c], Peter Renner [d], Dilworth Parkinson [e], Alexander Sinyukov [f], Hong Liang [a,g,*]

[a] Department of Materials Science & Engineering, Texas A&M University, College Station, TX 77843, USA
[b] Small Animal Clinical Sciences, Texas A&M University College of Veterinary Medicine & Biomedical Sciences, Texas A&M University, College Station, TX 77843, USA
[c] Department of Biomedical Sciences, Texas A&M University College of Dentistry, Dallas, TX 75246, USA
[d] Mike Walker '66 Department of Mechanical Engineering, Texas A&M University, College Station, TX 77843, USA
[e] Advanced Light Source, Lawrence Berkeley National Laboratory, Berkeley, CA 94720, USA
[f] Department of Physics & Astronomy, Texas A&M University, College Station, TX 77843, USA
[g] J. Mike Walker '66 Department of Mechanical Engineering, Texas A&M University, College Station, TX 77843-3123, USA

ARTICLE INFO

Keywords:
Chewing
Dog tooth
Enamel
Nanomaterials
Coatings
Tooth wear

ABSTRACT

The objective of this research is to study the feasibility using nanomaterials to prevent and/or repair wear of teeth. Canine teeth have thin enamel prone to dental wear, causing pain, tooth loss, and infection. This research developed a new teeth repair agent based on the tribochemically active nanoparticles. The presence and properties of synthesized repair agents were evaluated after applying the repair agents by rubbing (simulated chewing) between extracted dog teeth. Polyether modified alpha-zirconium phosphate (α-ZrP) nanoparticles form a strong and durable protective layer on a canine tooth's enamel surface through chewing. The effectiveness of this protective film generation was enhanced by adding hydroxyapatite (HAp) nanoparticles into the repair agent. This protective film is up to 2 μm thick and has a hardness comparable to the enamel substrate. These results show that by chewing with the repair agent, the teeth are protected. The tomography result shows this repair agent also has the potential to mend cracks on the enamel surface. This research reports a novel approach to protect the wear of teeth. Nanoparticles promoted the generation of a protective film in situ during the chewing process. This nanomaterial can be the base of novel dental protective devices such as chewing toys or gums that preventing or reversing tooth wear and reducing the stress and cost of dental restoration operations.

1. Introduction

Tooth enamel is the hardest and most dense structure in the mammalian body. It serves to protect the interior of the tooth from the normal flora of the oral cavity and other harmful substances [1,2]. Although it is the hardest tissue in humans and animals [3–6], it can suffer damage from mechanical forces [7–12] and acidic solutions [13–16]. In dogs, the enamel layer is significantly thinner than in humans [17] and more prone to excessive wear and damage. This type of wear can result in dentin and pulp exposure causing significant oral pain, tooth loss, or periarticular and pulpal infections [18,19], leading to deterioration in quality of life and, in extreme cases, to be life threatening [13,20,21].

Recently, remineralization of damaged tooth enamel was presented as an alternative method to traditional dental operations [22–24]. These researchers utilized the bio-mineralization process that naturally presented in the dental environment [25–27]. Precursors to the nanoparticle hydroxyapatite were used to form the hard enamel tissue in vitro or in vivo [23,27]. Some examples of the precursors are casein phosphopeptide-stabilized amorphous calcium phosphate [28–30]; amelogenin with fluoride [31], and polydopamine with hydroxyapatite (HAP) [23]. Unlike traditional dental treatments, this method repaired teeth with materials that were almost identical to the teeth themselves. However, like the natural biomineralization process, using the remineralization method required significant time (>24 h) to take effect [22,23,27]. This is a major limitation to the clinical application of this approach.

It has been reported that functionalized nanoparticles, when used as additives in a lubricant, could generate a protective film on a pair of rubbing surfaces. [32–36]. Subjecting these particles to frictional forces generate a film on the surface called tribofilm [33,37–40]. This film is harder than the original substrate surface and likely can protect the

* Corresponding author at: Mechanical Engineering, TAMU, College Station, TX 77843-3123, USA
E-mail address: hliang@tamu.edu (H. Liang).

https://doi.org/10.1016/j.biotri.2021.100168
Received 21 October 2020; Received in revised form 11 January 2021; Accepted 31 January 2021
Available online 8 February 2021

surface from future damage. Our recent research found that α-zirconium phosphate (α-ZrP) and sodium yttrium fluoride (NaYF4) were effective additives to form the tribofilm [40–43]. The α-ZrP nanoparticles have a unique layered structure which is held together via Van der Waals forces [44,45]. Under shear, chemical reactions between particle and surface are triggered, forming a protective layer on the surface [40,42]. This process may be attributed to the mechanical mixing during the sliding [46]. To date, repairing or preventing surface wear of teeth using the concept of tribofilms has not been reported [37,40], albeit the tribofilm in other biotribology systems such as hip-joint replacement was well studied [47]. This new method was inspired by the effectiveness and rapidity of tribochemical interactions between rubbing surfaces. This interaction can form a protective film more rapidly compared to current alternate remineralization methods.

2. Materials and methods

2.1. Repair material synthesis

The α-ZrP nanoparticles and HAP nanoparticles were synthesized using hydrothermal methods. For α-ZrP, 50 mL food grade 12 M phosphoric acid (Sigma Aldrich, St. Louis, USA) and 5 g zirconyl chloride octahydrate ($ZrOCl_2 \cdot 8H_2O$, Sigma Aldrich, St. Louis, USA) was mixed under constant stirring conditions. The mixture was then sealed in a polytetrafluoroethylene (PTFE) lined autoclave and moved to a 200°C oven for 24 h. The precursor of HAP was prepared with the following procedure: 12 mL 0.25 M calcium nitrate (Sigma Aldrich, St. Louis, USA) solution ($Ca(NO_3)_2$) was added dropwise into 20 mL 0.15 M disodium hydrogen phosphate (Na_2HPO_4, Sigma Aldrich, St. Louis, USA) solution under constant stirring at 50–60°C. The pH of this mixture was adjusted to 8–10 with ammonium hydroxide (Sigma Aldrich, St. Louis, USA). This mixture was put in a PTFE lined autoclave and placed in a 160°C oven for 12 h. After the hydrothermal reactions, the products were washed with deionized (DI) water and retrieved by centrifugation three times. The washed nanoparticles were dried in a vacuum furnace at 70°C for 12 h. The synthesized α-ZrP was intercalated with polyether amine M-600 (Huntsman Corporation, Houston, TX, USA). The synthesized 1 mmol α-ZrP was first dispersed in 5 mL of DI water with an ultrasonic bath for 1 h, then 5 mL 0.4 M M-600 solution was added into the dispersion dropwise.

The repair agents, as pastes, were developed as a mixture of the HAP nanoparticles and M-600 amine intercalated α-ZrP. Particles of α-ZrP can form a tribofilm when being rubbed. The M-600 amine intercalation improves its performance in aqueous environment, and HAP nanoparticle added as a filler material. The synthesized dispersion of intercalated α-ZrP was first mixed with the HAP nanoparticles. The amount of HAP nanoparticles used in mass ratios to α-ZrP before intercalation was 0:1, 0.25:1, 0.5:1 and 1:1 (the produced repair agents were labeled as S0, S2.5, S5 and S10). The products were centrifuged for 10 min. After the centrifuge process, the supernatants were removed by tilting the tubes, and the precipitates were retrieved. These precipitates were used in the tribo-mastication process described in the following sections.

2.2. Pin and disc tooth preparation

Dog canine teeth were used to create both "disc" teeth and "pin" teeth for the experiment. All dog canine teeth were procured from postmortem extractions from dogs used in unrelated studies. Before the experiment, all the teeth were washed in hydrogen peroxide (H_2O_2) and DI water. Any residual soft tissue (dental gum) was removed with a small knife.

To make the disc teeth, each canine tooth was first sealed in epoxy resin with the chewing contact surface exposed. Then, the enamel of this surface was carefully shaved flat, ground smooth with sandpaper and polished with a 3 μm grit diamond paste. No dentin was exposed during this process. This polishing process created one flat surface on each tooth to simulate mechanically worn or damaged enamel and created a reference surface for film thickness measurement. This process was repeated for five times to make 5 flat surfaces on five "disc" teeth Five teeth, each with one flat disc areas were created. The "pin" teeth were untreated dog canine teeth.

2.3. Experimental procedure

To simulate the chewing and grinding motion of teeth, a rubbing process was used. This process was conducted on a pin-on-disc tribometer (CSM Instruments, Needham, Massachusetts). The set-up of this rubbing mastication experiment is illustrated in Fig. 1. In every rubbing mastication experiment, two freshly prepared dog canine teeth were used, one configured as a pin, and the other as the disc. The normal force on the pin was 1 Newton (N). This force generates an approximate pressure of 100 MPa on the contact area, which is similar to the pressure a tooth experiences when chewing on hard food such as bones [48]. The "pin" tooth was moved with a sinusoidal reciprocal motion on the disc tooth with an amplitude of 2 mm and a maximum speed of 1 cm/s. Approximately 0.005 mL of repair agent paste was placed between the teeth before the rubbing-mastication process started. Because the repair agent is a paste containing water, this simulated "chewing" was analog to a wear test with water-based lubricant. However, it differs from a wear test because the material was added to the surface instead of removed from the surface. The motion was terminated after 100 cycles. This number of cycles was chosen to demonstrate that the protective film can form in a short chewing session when the repair agent was used clinically. After the process, samples were washed with DI water and air-dried. The repair agents (S0, S2.5, S5, and S10) were tested with this rubbing-mastication process before interferometry and atomic force microscopy (AFM) observation. Each set of tests with each material were carried out on a new pair of teeth and repeated five times at adjacent new locations. In total, five pairs were used, which included four repair agents. The disc tooth was used for surface characterization in order to quantify the repair outcome.

2.4. Characterization

After rubbing experiments, surfaces were examined using interferometry, atomic force microscope, and Raman spectroscopic techniques. After the rubbing-mastication process, the effect of each repair agent on all "disc" samples were characterized. The formed film morphology and microstructure were characterized by an interferometer (Zygo NewView 600, Zygo Corp, Berwyn, PA) and atomic force microscopy (AFM, Nano-R2, Pacific Nanotechnology, Santa Clara, CA) using close-contact mode. The interferometer mapped the topographic information of samples

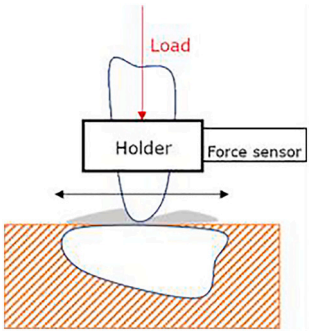

Fig. 1. The rubbing-mastication process. Two canine teeth were used in this setup, one as the "disc" (bottom) and one as the "pin" (top). The "disc" tooth was sealed in epoxy (dashed block) with surface enamel polished. The "pin" tooth was pressed down and rubbed against the "disc" tooth with a reciprocal motion. The grey area indicates the location of accumulation of the repair agents during rubbing.

optically. A heightmap was generated for each sample based on the monochromatic light interference. This heightmap provides an accurate measurement of the protective film thickness. The AFM also generated a heightmap for each sample with a tiny probe. That prob. interacts with the surface-force of samples. The heightmap and a phase map were generated by tracing that interaction. The Raman spectrum result of the repair film was collected with an iHR550 Spectrometer (HORIBA Scientific, Edison, NJ) with a 532 nm laser. The photon of the laser can inelastically scatter by chemical groups inside the surface layer of a sample. The wavelength of the scattered photons was detected with a digital controlled spectroscope. Two spectrums were collected, one from the repair film, the other from the polished tooth surface. Data collected from those instruments were plotted with python. All method described above are non-destructive and requires no further treatment of the samples.

2.5. Scratch test

To test if the newly created protective film was resistant to removal and to evaluate the mechanical strength of the protective film, a simple scratch test was preformed on the tooth sample (S5) that had visible film formed. The repair agent S5 was chosen because it generated the best thick protective film. The same tribometer with a steel needle was used to perform this scratch test. The needle was pressed against the tooth disc sample with 1 N force and scratched across the formed repair film and across exposed enamel manually.

2.6. Micro tomography

To examine the durability of repair film coverage on teeth, the "pin" teeth were analyzed with Synchrotron micro X-ray CT (μ-XCT). For this experiment, a new rubbing-mastication experiment was conducted. In this test, the tooth repair agent S5 was used with new "pin" and "disc" tooth samples. The S5 agent was chosen for the same reason as for the scratch test. The μ-XCT experiments were performed on the the Beam line 8.3.2 instrument at Lawrence Berkeley National Laboratory. All samples were imaged with a LuAG:Ce scintillator. Tomographic reconstruction was conducted using Xi-CAM with a tomopy tomography plugin.

The imaging of the coatings from all experimental films and controls was accomplished using the dual energy k-edge technique [49–51]. Before the test, the illuminating x-ray energy was calibrated to the x-ray absorption edge of the Zr with a pure α-ZrP nanoparticle sample. As illustrated in Fig. 2, the x-ray absorption by Zr element jumps around 18 KeV. Two illuminating energies were used to take two separate tomographic images of the same sample: 18.2 KeV and 17.8 KeV. From Fig. 2, when the sample was illuminated with 17.8 KeV, the Zr element will be brighter than when illuminated with 18.2 KeV. Thus, a simple subtraction between the two data sets can reveal the distribution of the Zr element, which demonstrates the distribution of the repair film. The data collected from these experiments were then rendered with Avizo software (Thermo Fisher Scientific, Waltham, MA).

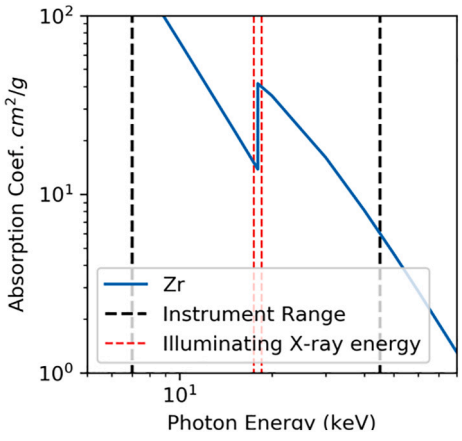

Fig. 2. The x-ray mass attenuation coefficient for Zr. The data used in this plot was collected from the National Institute of Standards and Technology database (NIST).

3. Results

3.1. Interferometry

Repair films were formed by the rubbing-mastication process for all repair agents. The interferometer topographic image is shown in Fig. 3. These figures show that the polishing process does provide a good reference surface under the film. Simulated chewing with the different repair agents generated protective films with different coverage and thickness ranging from 100 nm to 1 μm (orange to red range in Fig. 3). The coefficient of friction measured from those tests was 0.2. Where no repair material was present the baseline height of the enamel is yellow and where 100 nm to 1 μm of enamel was removed by polishing the color is green. The repair agent S0 resulted a continuous but thin film, while the repair agent S1 resulted in a lumpy but thick film. The repair agents S2.5 and S5 produced a film with better film coverage and film thickness compare to both S0 and S10. Compare to protective film formed with S2.5, the protective film formed by S5 was more continuous. Therefore, we concluded that the repair agent that produced the best result in terms of coverage and thickness was S5.

3.2. Atomic force microscopy (AFM)

The AFM analysis revealed the micro-structure of the intercalated α-ZrP repair films. Here the result from repair agent S0 which was pure intercalated α-ZrP and the repair agent S5 which have the best performance were shown (Fig. 4). In Fig. 4, the AFM height and phase map of the repair films in Fig. 3a and c are shown. The repair film generated with S0 contained many flaky particles on the surface with a size around 100 nm (Fig. 4a, b). The repair film generated with S5 showed a surface consisting of granular particles with a size around 50 nm (Fig. 4b, c).

3.3. Ramen spectroscopy

Raman analysis showed only two peaks for both tooth enamel and the repair films (Fig. 5). This figure plots the light intensity versus the light wavelength change due to Raman shift. This Raman shift was caused by the absorption and emission of photons by the chemical structure of the repair agents. In Fig. 5, two peaks were observed, one on the protective films and one on the enamel, both of them resulted from the $-PO_4$ group [45]. No additional chemicals were detected from the Raman spectrum, meaning that there are no other phospho- related chemical groups present on the sample surfaces.

3.4. Scratch test

In the scratch test, the generated films' scratch resistance was equal to or higher than the enamel of the tooth itself (Fig. 6). The scratches from the steel needle caused a loss of materials from both the tooth surface and the repair film surface. However, the repair film was not removed or exfoliated back to the depth of the sample's surface despite the scratching. Compared to the deep groove scratched onto the unprotected enamel surface, this repair film showed good hardness and wear resistance. This indicated the tribofime is sufficiently durable to protect the tooth surface.

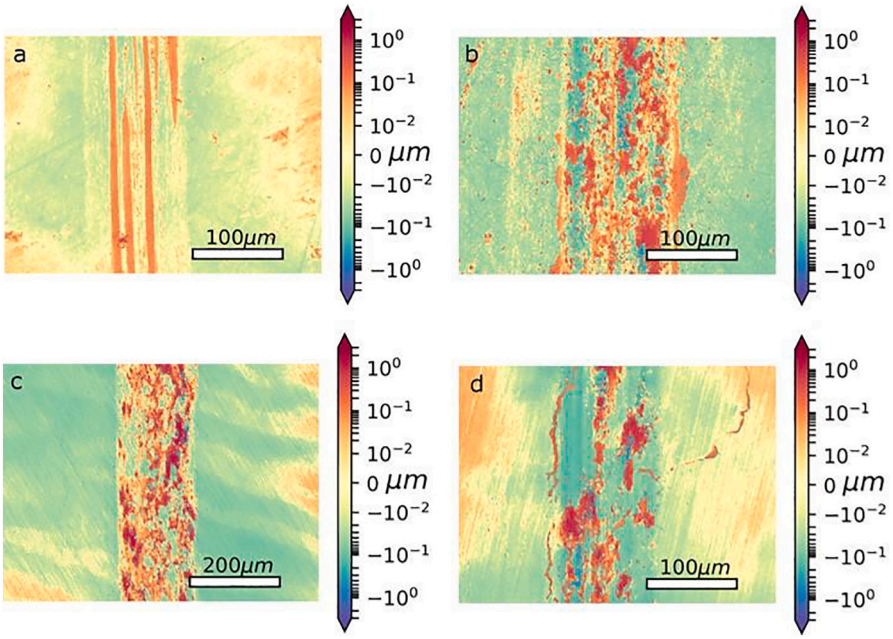

Fig. 3. The interferometer image of the enamel surface after the rubbing-mastication process with repair agent, S0(a), S2.5(b), S5(c) and S10 (d).

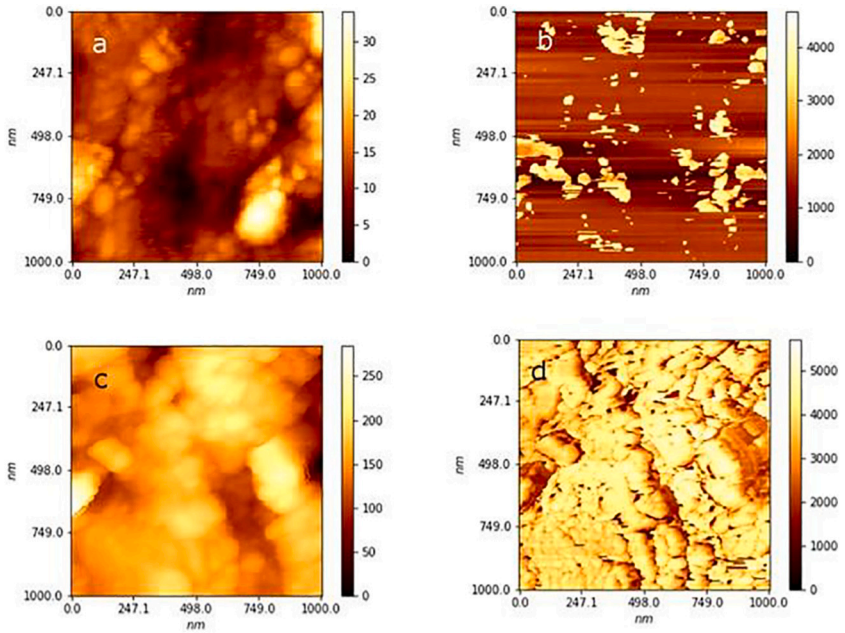

Fig. 4. The AFM height (a,c) and phase (b,d) image of the repair film generated with S0 (a,b) and S5(c,d). The unit of the color bars in a,c was nm, in b,d it was mV.

3.5. Synchrotron micro X-ray computed tomography

The appearance of a crack on the tip of one of the "pin" teeth allowed characterization of the depth of penetration of the repair material into the enamel instead of only on the surface using micro X-ray CT. In Fig. 7, the density distribution of the Zr element was overlaid on the reconstructed tooth image. This "pin" tooth was used in the rubbing-mastication process with the S5 agent. On the contact surface, a film was formed that wrapped around the tip of the tooth. In addition to that, the Zr element was detected inside the cracks to a depth of about 2 μm.

4. Discussion

Tribomastication with all repair agents resulted in a protective film being added to the enamel. The lowest concentration of α-ZrP produced the thinnest film, which also appeared as flakes on the surface of the enamel. The highest concentration of α-ZrP produced the thickest film but the distribution was very uneven. A pilot assessment of whether the film could be scratched off revealed that this film was resistant to scratching and that the generation of this film prevented wear on the tooth. The thickness and coverage of this repair film was controlled by manipulating the amount of HAP nanoparticles. With increased amounts of HAP, the thickness of the generated repair film was increased. With repair agent S0, the film thickness was only around 100 nm, but

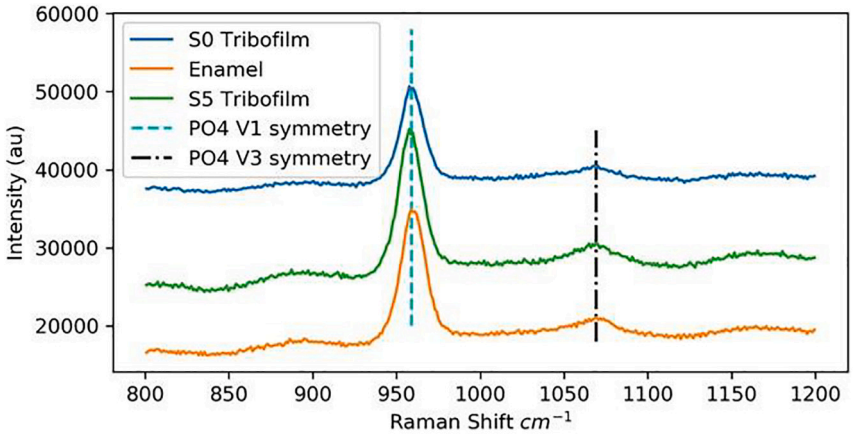

Fig. 5. The Raman spectra collected from the enamel surface and the repair film generated from S0 and S5. Two peaks resulted from the phosphate groups.

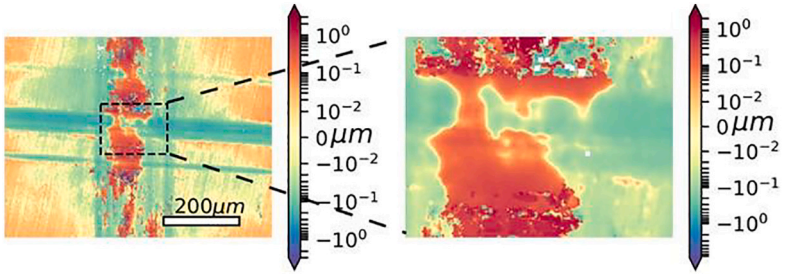

Fig. 6. The scratch test of the repair film generated by S5. The red color shows the repair film. After the scratch test, part of the film is still present while a deep groove was formed on the enamel surface next to the repair film. (For interpretation of the references to color in this figure legend, the reader is referred to the web version of this article.)

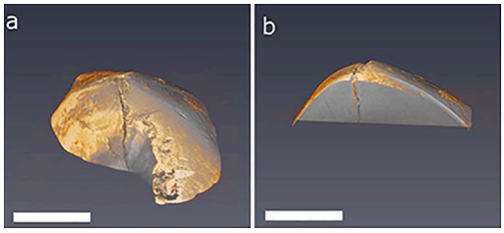

Fig. 7. The 3D rendering of the "pin" tooth after the rubbing-mastication process with repair agent S5. The distribution of the Zr element calculated from the dual energy k-edge technique was rendered as a golden color. a) the tip of the tooth. b) the cross-sectional rendering showing the repair agent had entered the surface crack. Scale bar length is 2 μm.

increased to 2 μm when the HAP:ZrP mass ratio was increased to 1:1 in the case of S10. The coverage of the repair film was also changed by this mass ratio. In the case of S0, a continuous film was produced and the sample S2.5 and S5 generated repair films that almost fully covered the wear track. Furthermore, when the ratio of α-ZrP and HAP increased to 1:2 in mass ratio, the repair film did not form at all. The addition of too much HAP nanoparticles caused the material to lose its rubbing-film forming properties. Because of this, we concluded that the S5 is a good compromise between film coverage and film thickness.

The AFM result provided some insight to the mechanism of the protective film generation. The particle size observed under AFM images (100 nm) were smaller than the α-ZrP size in the repair agent (1 μm) [43]. This means the generation of a protective film was not a direct deposition of the α-ZrP particles. Because the intercalation process decreased the Van der Waals force between the α-ZrP layers [41], they can be more readily exfoliated by the shear force during the rubbing-mastication process. These exfoliated functionalized 2-dimensional sheets thus became the building blocks of the repair film. The inclusion of HAP nanoparticles not only changed the micro-structure of the resulting repair film, but instead of a flaky aggregation of particles, a more regular cellular like structure was formed. This cellular structure consisted of grains with almost identical sizes, very likely to be the HAP nanoparticles. The HAP nanoparticles survived the rubbing-mastication process and were "glued" together by the "sticky" M600 attached α-ZrP. This further explained why the inclusion of HAP nanoparticles increased the thickness of the film but decreased the coverage. The HAP nanoparticles therefore cannot form a repair film without the intercalated α-ZrP. Thus, the higher concentration of HAP decreased the possibility of intercalated α-ZrP contacting the tooth surface. In addition to that, the Raman spectra showed that the generated film did not introduce any foreign inorganic functional groups on the surface of the teeth. The tribo-chemical process was known to chemically alter the phosphate group [33]. Because this process occurred in an aqueous environment, the influence of frictional heat is unlikely.

Based on these results, we propose the following repair film forming mechanism for this tooth repair agent. For the pure intercalated α-ZrP, the nanoparticles were exfoliated and broken down by the rubbing-mechanical force. Then, the polymer chains attached to the exfoliated nanoparticles reattached those exfoliated layers under shear. When polymer chains were ground together by the mechanical force, the polymerization process occurred [52–54]. This mechanochemical polymerization process appears to be the driving force for the growth of the repair film. When HAP nanoparticles are introduced, the polymer chain further interacts with the HAP crystals and "glues" the HAP crystals onto the tooth surface, forming a thick coherent film. This cohesiveness of the formed protective film also provides one explanation for its good strength. The micro-CT results further indicated that this repair mechanism may work in the enamel surface cracks as well as on

the enamel surface.

The approach reported here has potential clinical applications. In particular, the ability to form a protective coating under mastication condition makes it a good candidate for alleviation of occlusal surface damage. We will continue to investigate in this in near future.

5. Conclusions

In this research, a simple one-step procedure to reduce wear and repair teeth was developed. The formation of a protective film was made possible through mechanical rubbing (chewing) of materials consisting of nanoparticles, polymers, and biomaterials for mineralization. After rubbing (simulated mastication) between two teeth, the tooth repair agent formed a film with a thickness up to 2 μm. The formed repair film has a hardness comparable to the enamel surface. In addition to surface repair, this new agent can enter cracks on the enamel surface. The formation of such protective films may be attributed to the affinity between the polyether and HAP with the tooth enamel. Other polyether modified nanoparticles may also have the potential to form a protective film on the enamel surface. The future work will focus on exploring the in vivo performance of the repairing method. Efforts will be made on evaluating the durability of the protective film in real life condations..

This research presents a new concept and method to prevent enamel wear or repair teeth through chewing.

Declaration of Competing Interest

The authors declare that they have no known competing financial interests or personal relationships that could have appeared to influence the work reported in this paper.

Acknowledgement

All dog canine teeth were procured from postmortem extractions from dogs used in unrelated studies at the Texas A&M University Veterinary Medical Teaching Hospital. All were discard teeth not identifiable with any patient data and therefore not subject to IRB approval.

This work was supported by the Texas A&M President's Excellence Fund under the Texas A&M Triads of transformation program.

References

[1] B.H. Colmery, Composite restorative dentistry, Vet. Clin. Small Anim. Pract. 28 (1998) 1261–1271.
[2] B.A. Greenfield, Enamel defect restoration of the left mandibular first molar tooth, J. Vet. Dent. 29 (2012) 36–43.
[3] L.H. He, M.V. Swain, Enamel—a "metallic-like" deformable biocomposite, J. Dent. 35 (2007) 431–437, https://doi.org/10.1016/j.jdent.2006.12.002.
[4] D. Bajaj, D.D. Arola, On the R-curve behavior of human tooth enamel, Biomaterials. 30 (2009) 4037–4046, https://doi.org/10.1016/j.biomaterials.2009.04.017.
[5] J.J.-W. Lee, P.J. Constantino, P.W. Lucas, B.R. Lawn, Fracture in teeth—a diagnostic for inferring bite force and tooth function, Biol. Rev. 86 (2011) 959–974, https://doi.org/10.1111/j.1469-185X.2011.00181.x.
[6] S. Roy, B. Basu, Mechanical and tribological characterization of human tooth, Mater. Charact. 59 (2008) 747–756, https://doi.org/10.1016/j.matchar.2007.06.008.
[7] M. Addy, R.P. Shellis, Interaction between attrition, abrasion and erosion in tooth wear, Dent. Eros. 20 (2006) 17–31, https://doi.org/10.1159/000093348.
[8] D. Bajaj, A. Nazari, N. Eidelman, D.D. Arola, A comparison of fatigue crack growth in human enamel and hydroxyapatite, Biomaterials. 29 (2008) 4847–4854, https://doi.org/10.1016/j.biomaterials.2008.08.019.
[9] L.H. He, M.V. Swain, Contact induced deformation of enamel, Appl. Phys. Lett. 90 (2007) 171916, https://doi.org/10.1063/1.2450649.
[10] D. Rios, H.M. Honório, A.C. Magalhães, M.A.R. Buzalaf, R.G. Palma-Dibb, M.A. de Machado, S.M.B. da Silva, Influence of toothbrushing on enamel softening and abrasive wear of eroded bovine enamel: an in situ study, Braz, Oral Res. 20 (2006) 148–154, https://doi.org/10.1590/S1806-83242006000200011.
[11] R. Lewis, R.S. Dwyer-Joyce, Wear of human teeth: a tribological perspective, Proc. Inst. Mech. Eng. Part J J. Eng. Tribol. 219 (2005) 1–18, https://doi.org/10.1243/1350650053295394.
[12] L.C. Levitch, J.D. Bader, D.A. Shugars, H.O. Heymann, Non-carious cervical lesions, J. Dent. 22 (1994) 195–207, https://doi.org/10.1016/0300-5712(94)90107-4.
[13] M.A.R. Buzalaf, A.R. Hannas, M.T. Kato, Saliva and dental erosion, J. Appl. Oral Sci. 20 (2012) 493–502, https://doi.org/10.1590/S1678-77572012000500001.
[14] N.X. West, A. Joiner, Enamel mineral loss, J. Dent. 42 (2014) S2–S11, https://doi.org/10.1016/S0300-5712(14)50002-4.
[15] R. Cheng, H. Yang, M. Shao, T. Hu, X. Zhou, Dental erosion and severe tooth decay related to soft drinks: a case report and literature review, J Zhejiang Univ Sci B 10 (2009) 395–399, https://doi.org/10.1631/jzus.B0820245.
[16] D. Palamara, J.E.A. Palamara, M.J. Tyas, M. Pintado, H.H. Messer, Effect of stress on acid dissolution of enamel, Dent. Mater. 17 (2001) 109–115, https://doi.org/10.1016/S0109-5641(00)00047-6.
[17] S.E. Holmstrom, P.F. Fitch, E.R. Eisner, Veterinary Dental Techniques for the Small Animal Practitioner, Elsevier Health Sciences, 2004.
[18] R.F. Majewski, C.W. Snyder, J.E. Bernat, Dental emergencies presenting to a children's hospital, ASDC J. Dent. Child. 55 (1988) 339–342.
[19] B. Monse, R. Heinrich-Weltzien, H. Benzian, C. Holmgren, W.V.P. Helderman, PUFA – an index of clinical consequences of untreated dental caries, Community Dent. Oral Epidemiol. 38 (2010) 77–82, https://doi.org/10.1111/j.1600-0528.2009.00514.x.
[20] J.H. Nunn, Prevalence of dental erosion and the implications for oral health, Eur. J. Oral Sci. 104 (1996) 156–161, https://doi.org/10.1111/j.1600-0722.1996.tb00064.x.
[21] R.S. Lacruz, S. Habelitz, J.T. Wright, M.L. Paine, Dental enamel formation and implications for oral health and disease, Physiol. Rev. 97 (2017) 939–993, https://doi.org/10.1152/physrev.00030.2016.
[22] N.J. Cochrane, F. Cai, N.L. Huq, M.F. Burrow, E.C. Reynolds, New approaches to enhanced remineralization of tooth enamel, J. Dent. Res. 89 (2010) 1187–1197, https://doi.org/10.1177/0022034510376046.
[23] Y.-Z. Zhou, Y. Cao, W. Liu, C.H. Chu, Q.-L. Li, Polydopamine-induced tooth remineralization, ACS Appl. Mater. Interfaces 4 (2012) 6901–6910, https://doi.org/10.1021/am302041b.
[24] G. Walker, F. Cai, P. Shen, C. Reynolds, B. Ward, C. Fone, S. Honda, M. Koganei, M. Oda, E. Reynolds, Increased remineralization of tooth enamel by milk containing added casein phosphopeptide-amorphous calcium phosphate, J. Dairy Res. 73 (2006) 74–78.
[25] J. Arends, J.M. Ten Cate, Tooth enamel remineralization, J. Cryst. Growth 53 (1981) 135–147, https://doi.org/10.1016/0022-0248(81)90060-9.
[26] J. Hicks, F. Garcia-Godoy, C. Flaitz, Biological factors in dental caries: role of saliva and dental plaque in the dynamic process of demineralization and remineralization (part 1), J. Clin. Pediatr. Dent. 28 (2004) 47–52, https://doi.org/10.17796/jcpd.28.1.yg6m443046k50u20.
[27] H. Cölfen, A crystal-clear view, Nat. Mater. 9 (2010) 960–961, https://doi.org/10.1038/nmat2911.
[28] M. Oshiro, K. Yamaguchi, T. Takamizawa, H. Inage, T. Watanabe, A. Irokawa, S. Ando, M. Miyazaki, Effect of CPP-ACP paste on tooth mineralization: an FE-SEM study, J. Oral Sci. 49 (2007) 115–120, https://doi.org/10.2334/josnusd.49.115.
[29] T. Sitthisettapong, P. Phantumvanit, C. Huebner, T. DeRouen, Effect of CPP-ACP paste on dental caries in primary teeth: a randomized trial, J. Dent. Res. 91 (2012) 847–852, https://doi.org/10.1177/0022034512454296.
[30] J. Jayarajan, P. Janardhanam, P. Jayakumar, Deepika, efficacy of CPP-ACP and CPP-ACPF on enamel remineralization - an in vitro study using scanning electron microscope and DIAGNOdent®, Indian J. Dent. Res. 22 (2011) 77, https://doi.org/10.4103/0970-9290.80001.
[31] Y. Fan, Z. Sun, J. Moradian-Oldak, Controlled remineralization of enamel in the presence of amelogenin and fluoride, Biomaterials. 30 (2009) 478–483, https://doi.org/10.1016/j.biomaterials.2008.10.019.
[32] H. Spikes, The history and mechanisms of ZDDP, Tribol. Lett. 17 (2004) 469–489, https://doi.org/10.1023/B:TRIL.0000044495.26882.b5.
[33] J. Zhang, H. Spikes, On the mechanism of ZDDP antiwear film formation, Tribol. Lett. 63 (2016) 24, https://doi.org/10.1007/s11249-016-0706-7.
[34] H. Kato, K. Komai, Tribofilm formation and mild wear by tribo-sintering of nanometer-sized oxide particles on rubbing steel surfaces, Wear. 262 (2007) 36–41.
[35] H.L. Yu, Y. Xu, P.J. Shi, B.S. Xu, X.L. Wang, Q. Liu, H.M. Wang, Characterization and nano-mechanical properties of tribofilms using Cu nanoparticles as additives, Surf. Coat. Technol. 203 (2008) 28–34.
[36] W. Dai, B. Kheireddin, H. Gao, H. Liang, Roles of nanoparticles in oil lubrication, Tribol. Int. 102 (2016) 88–98.
[37] N.N. Gosvami, J.A. Bares, F. Mangolini, A.R. Konicek, D.G. Yablon, R.W. Carpick, Mechanisms of antiwear tribofilm growth revealed in situ by single-asperity sliding contacts, Science. 348 (2015) 102–106, https://doi.org/10.1126/science.1258788.
[38] W. Dai, Y. Chen, K. Lee, A.M. Sinyukov, M. Alkahtani, P.R. Hemmer, H. Liang, In situ investigation of the growth of a tribofilm consisting of NaYF4 fluorescent nanoparticles, Tribol. Trans. (2017) 1–10.
[39] W. Dai, K. Lee, A.M. Sinyukov, H. Liang, Effects of vanadium oxide nanoparticles on friction and wear reduction, J. Tribol. 139 (2017), 061607.
[40] W. Dai, B. Kheireddin, H. Gao, Y. Kan, A. Clearfield, H. Liang, Formation of anti-wear tribofilms via α-ZrP nanoplatelet as lubricant additives, Lubricants. 4 (2016) 28.
[41] H. Xiao, W. Dai, Y. Kan, A. Clearfield, H. Liang, Amine-intercalated α-zirconium phosphates as lubricant additives, Appl. Surf. Sci. 329 (2015) 384–389, https://doi.org/10.1016/j.apsusc.2014.12.061.
[42] X. He, H. Xiao, H. Choi, A. Díaz, B. Mosby, A. Clearfield, H. Liang, α-Zirconium phosphate nanoplatelets as lubricant additives, Colloids Surf. A Physicochem. Eng. Asp. 452 (2014) 32–38, https://doi.org/10.1016/j.colsurfa.2014.03.041.

[43] Y. Chen, X. Wang, A. Clearfield, H. Liang, Anti-galling effects of α-zirconium phosphate nanoparticles as grease additives, J. Tribol. 141 (2018) 031801–031806, https://doi.org/10.1115/1.4041538.
[44] A. Clearfield, S.D. Smith, The crystal structure of zirconium phosphate and the mechanism of its ion exchange behavior, J. Colloid Interface Sci. 28 (1968) 325–330, https://doi.org/10.1016/0021-9797(68)90136-7.
[45] J.M. Troup, A. Clearfield, Mechanism of ion exchange in zirconium phosphates. 20. Refinement of the crystal structure of alpha-zirconium phosphate, Inorg. Chem. 16 (1977) 3311–3314, https://doi.org/10.1021/ic50178a065.
[46] D.A. Rigney, S. Karthikeyan, The evolution of tribomaterial during sliding: a brief introduction, Tribol. Lett. 39 (2010) 3–7, https://doi.org/10.1007/s11249-009-9498-3.
[47] M.T. Mathew, C. Nagelli, R. Pourzal, A. Fischer, M.P. Laurent, J.J. Jacobs, M. A. Wimmer, Tribolayer formation in a metal-on-metal (MoM) hip joint: an electrochemical investigation, J. Mech. Behav. Biomed. Mater. 29 (2014) 199–212, https://doi.org/10.1016/j.jmbbm.2013.08.018.
[48] Y.N. Yeni, D.P. Fyhrie, A rate-dependent microcrack-bridging model that can explain the strain rate dependency of cortical bone apparent yield strength, J. Biomech. 36 (2003) 1343–1353, https://doi.org/10.1016/S0021-9290(03)00122-2.
[49] Y. Chen, C. Sanchez, Y. Yue, J.M. González, D.Y. Parkinson, H. Liang, Observation of two-dimensional yttrium oxide nanoparticles in mealworm beetles (*Tenebrio molitor*), J. Synchrotron Radiat. 23 (2016) 1197–1201.
[50] Y. Chen, C. Sanchez, Y. Yue, M. de Almeida, J.M. González, D.Y. Parkinson, H. Liang, Observation of yttrium oxide nanoparticles in cabbage (*Brassica oleracea*) through dual energy K-edge subtraction imaging, J. Nanobiotechnol. 14 (2016) 23, https://doi.org/10.1186/s12951-016-0175-z.
[51] Y. Chen, C. Sanchez, D.Y. Parkinson, H. Liang, Direct observation of lubricant additives using tomography techniques, Appl. Phys. Lett. 109 (2016), 041603, https://doi.org/10.1063/1.4960020.
[52] M. Hasegawa, Y. Akiho, Y. Kanda, Mechanochemical polymerization of methyl methacrylate initiated by the grinding of inorganic compounds, J. Appl. Polym. Sci. 55 (1995) 297–304, https://doi.org/10.1002/app.1995.070550213.
[53] M. Hasegawa, M. Kimata, S.-I. Kobayashi, Mechanochemical copolymerization of methyl methacrylate and styrene initiated by the grinding of quartz, J. Appl. Polym. Sci. 84 (2002) 2011–2017, https://doi.org/10.1002/app.10544.
[54] S.L. Craig, Mechanochemistry: a tour of force, Nature. 487 (2012) 176–177, https://doi.org/10.1038/487176a.